Arch. Pharm. Chem. Life Sci. 2016, *349*, 91–103

ARCH PHARM
Archiv der Pharmazie

Full Paper

Linker-Region Modified Derivatives of the Deoxyhypusine Synthase Inhibitor CNI-1493 Suppress HIV-1 Replication

Marcus Schröder[1], Adrian Kolodzik[2], Björn Windshügel[2], Marcel Krepstakies[3], Poornima Priyadarshini[3], Philip Hartjen[4], Jan van Lunzen[4], Matthias Rarey[2], Joachim Hauber[3], and Chris Meier[1]

[1] Institute of Organic Chemistry, Department of Chemistry, Faculty of Sciences, University of Hamburg, Hamburg, Germany
[2] ZBH Center for Bioinformatics, University of Hamburg, Hamburg, Germany
[3] Heinrich Pette Institute – Leibniz Institute for Experimental Virology, Hamburg, Germany
[4] Department of Medicine, Infectious Diseases Unit, University Medical Center Hamburg-Eppendorf, Hamburg, Germany

The inhibition of cellular factors that are involved in viral replication may be an important alternative to the commonly used strategy of targeting viral enzymes. The guanylhydrazone CNI-1493, a potent inhibitor of the deoxyhypusine synthase (DHS), prevents the activation of the cellular factor eIF-5A and thereby suppresses HIV replication and a number of other diseases. Here, we report on the design, synthesis and biological evaluation of a series of CNI-1493 analogues. The sebacoyl linker in CNI-1493 was replaced by different alkyl or aryl dicarboxylic acids. Most of the tested derivatives suppress HIV-1 replication efficiently in a dose-dependent manner without showing toxic side effects. The unexpected antiviral activity of the rigid derivatives point to a second binding mode as previously assumed for CNI-1493. Moreover, the chemical stability of CNI-1493 was analysed, showing a successive hydrolysis of the imino bonds. By molecular dynamics simulations, the behaviour of the parent CNI-1493 in solution and its interactions with DHS were investigated.

Keywords: Anti-HIV activity / Deoxyhypusine synthase / DHS / eIF-5A / Inhibitor synthesis

Received: September 14, 2015; Revised: December 2, 2015; Accepted: December 4, 2015

DOI 10.1002/ardp.201500323

Additional supporting information may be found in the online version of this article at the publisher's web-site.

Introduction

The eukaryotic initiation factor 5A (eIF-5A) is unique, since it is to date the only known cellular protein that contains the unusual amino acid hypusine (N^{ε}-[4-amino-2-hydroxybutyl]-lysine). This post-translational spermidine-dependent modification is required for eIF-5A activity and occurs at Lys50 in the human 154-amino acid eIF-5A protein [1, 2]. Hypusination of eIF-5A is catalysed by the sequential action of deoxyhypusine synthase (DHS) and deoxyhypusine hydroxylase (DOHH; Fig. 1). DHS mediates the transfer of the aminobutyl moiety of spermidine to the ε-NH_2 group of Lys50 to form an intermediate reaction substrate. This still inactive intermediate is subsequently hydroxylated by DOHH, resulting in the active hypusine-modified protein.

Although eIF-5A has been initially described as an 'initiation' factor of the protein synthesis [3, 4], more recent studies demonstrated that eIF-5A rather promotes the elongation step of translation [5, 6]. Interestingly, this eIF-5A activity occurs in mammalian cells particularly during cellular stress [7, 8], which may suggest that hypusinated eIF-5A acts in the translation of a small and distinct subset of cellular transcripts. In addition to affecting translational elongation, in higher eukaryotes eIF-5A also participates in the nucleocytoplasmic

Correspondence: Prof. Chris Meier, Institute of Organic Chemistry, Department of Chemistry, Faculty of Sciences, University of Hamburg, Martin-Luther-King-Platz 6, 20146 Hamburg, Germany.
E-mail: chris.meier@chemie.uni-hamburg.de
Fax: +49 40 428385592

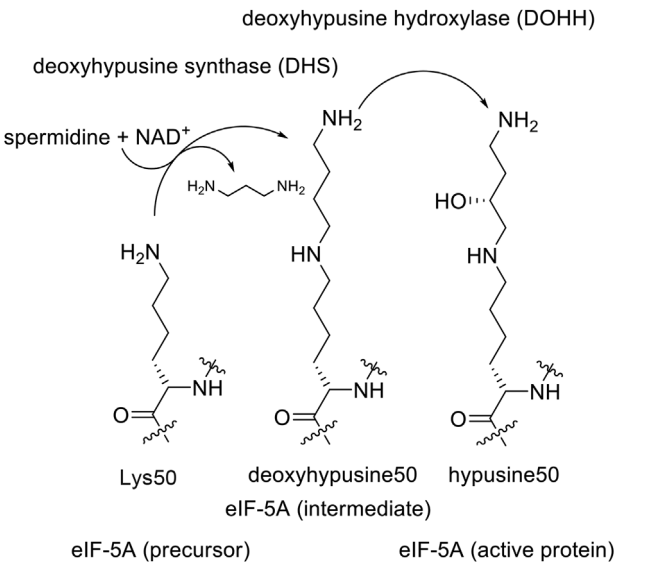

Figure 1. *In vivo* activation of eIF-5A catalysed by DHS and DOHH.

translocation of specific mRNAs. For example, independent evidence has been provided demonstrating that eIF-5A regulates the nuclear exit of cellular transcripts via the CRM1/exportin1 pathway, particularly encoding the surface protein CD83 [9, 10] or inducible nitric oxide synthase (iNOS) [11]. It is noted, however, that nuclear eIF-5A has been also reported to interact with XPO4/exportin4, another CRM1-unrelated transport receptor [12]. Nevertheless, in HIV-1 infection eIF-5A serves as a cellular cofactor of the essential viral regulatory protein Rev, thereby promoting the CRM1-dependent nuclear export of unspliced and incompletely spliced retroviral mRNAs [13, 14]. Moreover, it was demonstrated that inhibition of DHS by small-molecular weight inhibitors or RNA interference (RNAi) suppressed the cytoplasmic accumulation of Rev-regulated viral transcripts and, in consequence, the formation of virus progeny [15, 16]. Thus, pharmacological interference with DHS activity may provide a novel strategy to efficiently inhibit HIV-1 replication, particularly viral strains with high-level resistance to inhibitors of current combinational antiretroviral therapy (cART) [17]. In particular, the guanylhydrazone CNI-1493 (compound **1** in Fig. 2, the INN is semapimod), an experimental anti-inflammatory drug [18], has been shown *in vitro* as well as in living cells to be an efficient DHS inhibitor with activity not only against HIV [15, 19] but also against other diseases or pathogens [20, 21]. Concerning the ability of CNI-1493 to cross cell membranes, it was shown that fetuin can mediate the cellular uptake in macrophages [22]. Due to its size, CNI-1493 can not fit in the active site of the DHS. A recently solved co-crystal structure of CNI-1493 bound to DHS revealed that CNI-1493 was bound at the end of a narrow channel at the surface of the protein. In the bound form, the molecule adopted a U-shape structure with the guanidine-residues interacting

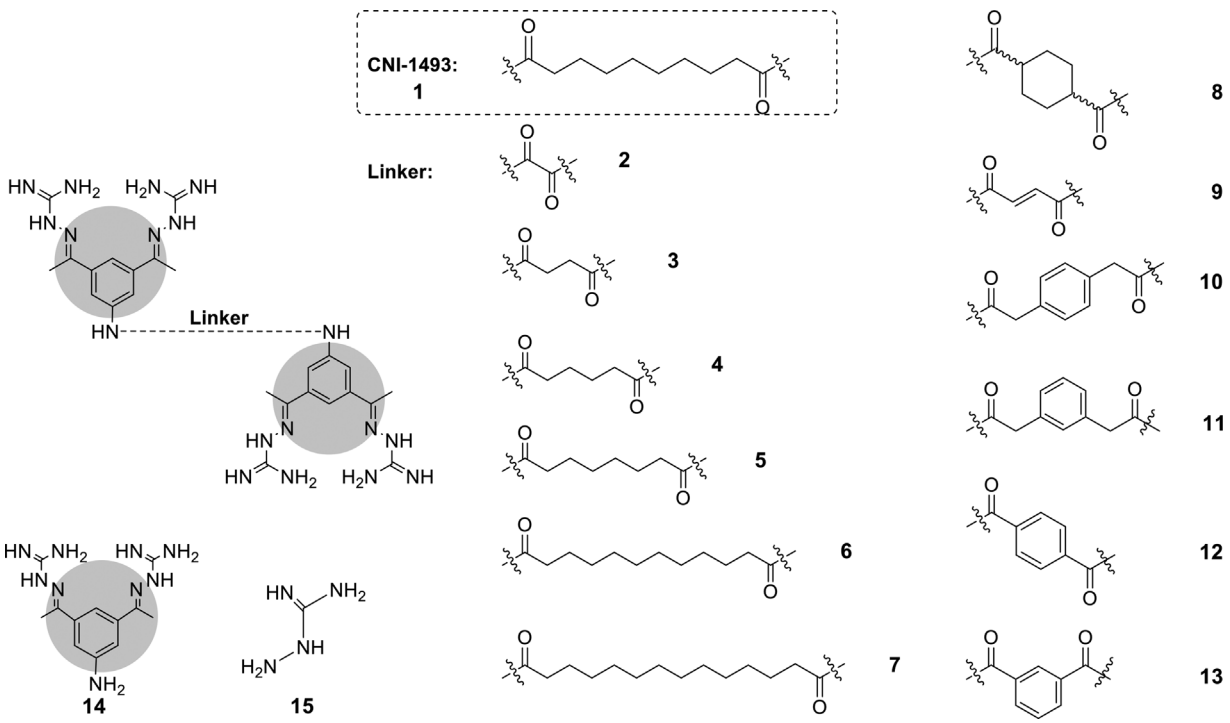

Figure 2. Summary of the synthesised CNI-1493 analogues **2**–**15**.

with the protein side chains [23]. The combined data provided the starting point for a structure-activity-relationship study to develop novel inhibitors of DHS that may, as outlined before, be particularly useful in the treatment of diseases inflicted by otherwise cART-resistant HIV-1. We report the synthesis and *in vitro* test of various compounds derived from CNI-1493, including the analysis of their DHS inhibitory capacity as well as their effects on cellular metabolism and HIV-1 replication. Moreover, the corresponding energy-minimised structures of these compounds were superposed with that of CNI-1493 and molecular dynamics simulation was employed for modelling the binding between CNI-1493 and the DHS.

Results and discussion

Synthesis of the CNI-1493 analogues

In order to analyse the structural requirements for inhibition of DHS by CNI-1493 (**1**), the CNI-1493 structure was varied by replacing the alkyl chain with more rigid linkers or simply either shortened or elongated the alkyl chain (Fig. 2).

In summary, a series of CNI-1493 derivatives **2**–**14** were synthesised for a structure-activity-relationship study. For this small library of CNI-1493 analogues, an earlier reported synthetic approach was used starting from 5-nitro isophthalic acid **16**, whose nitro group serves as an amino group precursor [24, 25]. First, 5-nitro isophthalic acid **16** was converted into the corresponding dichloride **18** using thionyl chloride with a catalytic amount of DMF. In contrast to the procedure reported in the literature, the following reaction of **18** with diethyl magnesium malonate failed. Thus, in a one-pot reaction, sodium hydride was used for the deprotonation of diethylmalonate **17** before adding 5-nitro isophthaloyl dichloride **18** leading to an intermediate, which was not isolated but was directly reacted in a hydrolytic decarboxylation to 5-nitro-1,3-diacetylbenzene **19** (Scheme 1). The reduction of the nitro group to yield 3,5-diacetylaniline **20** was achieved by tin(II) chloride [25]. Compound **15** was commercially available.

The tetraketones **21**–**33** (Scheme 1) were prepared by reaction of **20** with the corresponding diacid dichlorides in dry CH_2Cl_2/pyridine according to a method from Bianchi et al. [26].

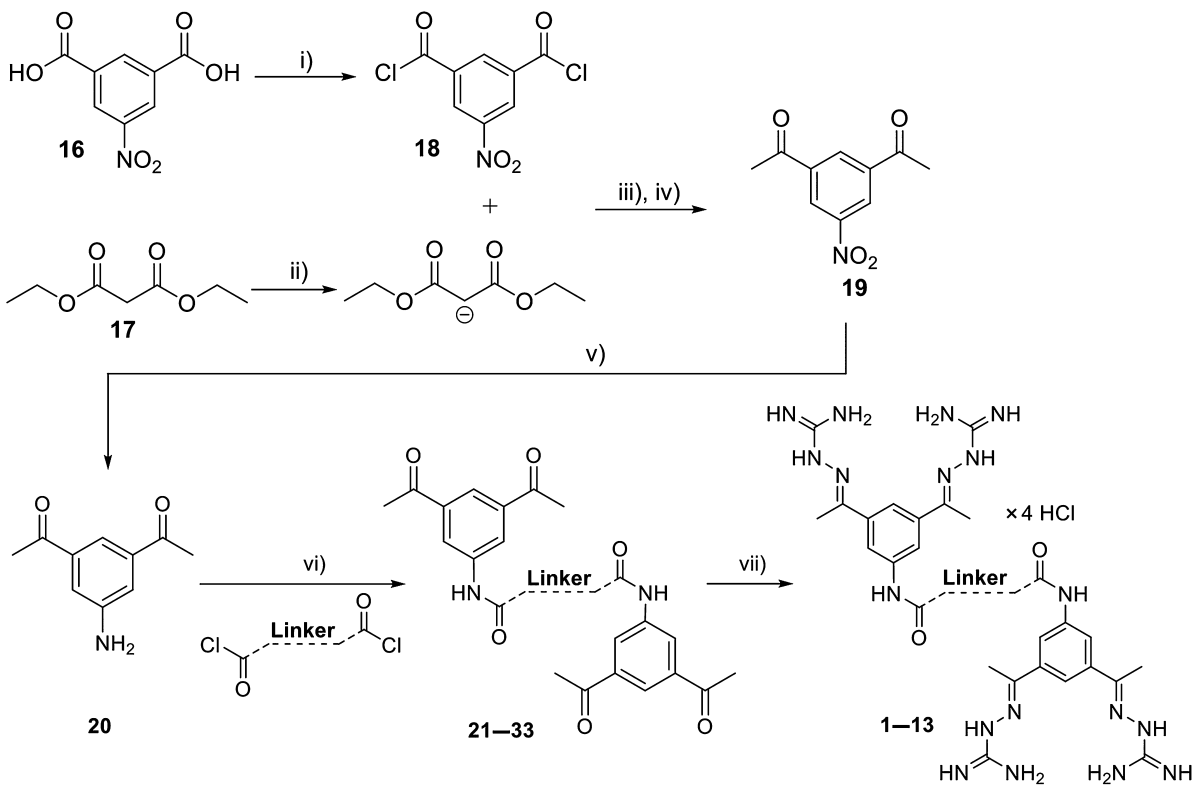

Scheme 1. Synthesis of 3,5-diacetylaniline **20** and its conversion to CNI-1493 (**1**) and the CNI-1493 analogues **2**–**13**. Reagents and conditions: i) $SOCl_2$, DMF, reflux, [N_2], 90 min; ii) NaH, THF, reflux, [N_2], 4 h; iii) THF, reflux, [N_2], 16 h; iv) AcOH/water/H_2SO_4, reflux, 3.5 h; i)–iv) 29%; v) $SnCl_2$, conc. HCl, 50°C, 15 min, 98%; vi) 0.5 eq. dicarboxylic acid chloride, 2.7 eq. pyridine, CH_2Cl_2, rt, [N_2], 2–15 h, 38–96%; vii) 5 eq. aminoguanidine hydrochloride, ethanol/water 9:1, conc. HCl, reflux, 3 h, 24–95%.

The final step was the conversion to the guanylhydrazone derivatives **1**–**14** using aminoguanidine hydrochloride in ethanol under acid catalysis [26]. As CNI-1493, all CNI-1493 analogues precipitated as pure compounds at −26°C and were isolated as their hydrochlorides by filtration and washing steps in yields from 24 to 95%.

Inhibition of the human DHS enzyme

In order to investigate the ability of the new compounds **2**–**14** to inhibit DHS, all compounds were tested in an enzymatic *in vitro* DHS assay. Therefore, the DHS reaction was simulated employing recombinant expressed eIF-5A and DHS together with the substrates NAD^+ and ^3H-labelled spermidine. The reaction was performed with the indicated concentrations of the derivatives **2**–**14** as well as with compound **15**, CNI-1493 (**1**) as a positive control or only DMSO as the negative control, respectively. As a measure for DHS activity, the relative amount of the transferred tritium-labelled aminobutyl residue from spermidine to eIF-5A was detected. As shown before, CNI-1493 (**1**) inhibited the DHS reaction in a concentration-dependent manner [15]. The inhibitory effect was greater than 90% at the highest tested concentration (5 μM). Interestingly, several of the CNI-1493 analogues showed a similar effect on the enzymatic DHS reaction (Fig. 3). Most of these active compounds belong to the group with an aliphatic linker (Fig. 3A). For **7** (linker contains 12 methylene groups), the alkyl linker may be too long for effective binding to DHS, which possibly explains the observed decrease in activity.

In compound **2**, the two head groups were directly linked whereas the linker lengths of the other compounds varied between two and twelve methylene groups. In comparison, CNI-1493 (**1**) contains a $(CH_2)_8$ chain as linker. The aminoguanidine moiety **15** alone, which was found in the spermidine pocket of the CNI-1493-DHS co-crystal structure, had no effect on DHS activity. Additionally, the truncated derivative **14** showed nearly no inhibitory effect on DHS. Among the CNI-1493 derivatives with a linker bearing a rigid aromatic residue compound **12**, in which the two head groups are linked in 4 positions of the phenyl ring, showed an activity similar to **1** (Fig. 3B).

The four most promising inhibitors from this series of the aliphatic and the aromatic linker class (Fig. 4) were further tested in a HIV infection assay.

Inhibition of HIV-1 replication in cell culture

DHS-inhibitor candidates **3**, **6**, **12** and **13** as well as CNI-1493 (**1**) as a positive control were tested in regard to their potential to inhibit the replication of HIV-1 in cell culture. For this purpose, PM1 cells were preincubated for 8–10 days in presence of the compounds at concentrations of 0.5, 1 and 2 μM or DMSO (solvent control) and then infected with the CCR5-tropic HIV-1 strain BaL. After further cultivation for 7 days, p24 antigen levels in the cell culture supernatants and cellular viability (measured by AlamarBlue staining) were determined.

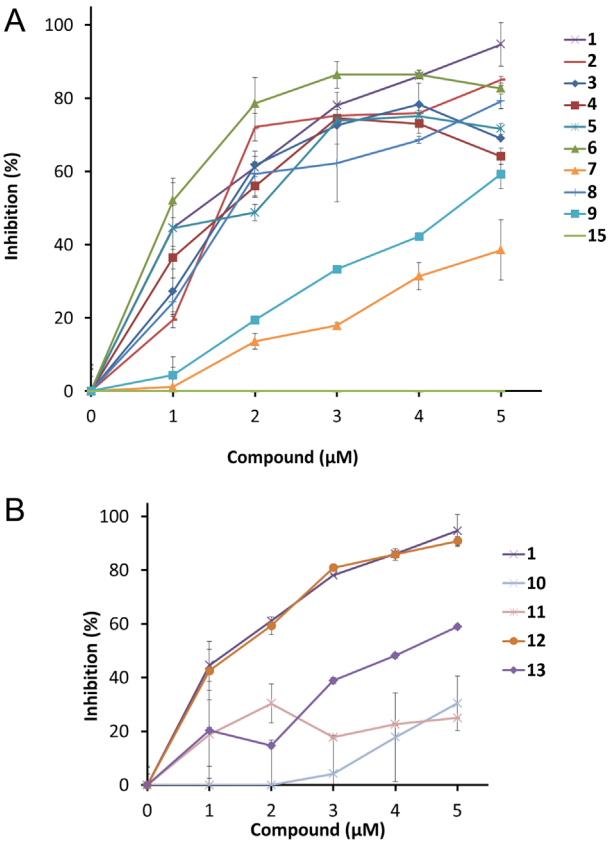

Figure 3. DHS inhibition assay with aliphatic CNI-1493 analogues (A) and with the aromatic CNI-1493 derivatives (B). CNI-1493 (**1**) was used as a reference.

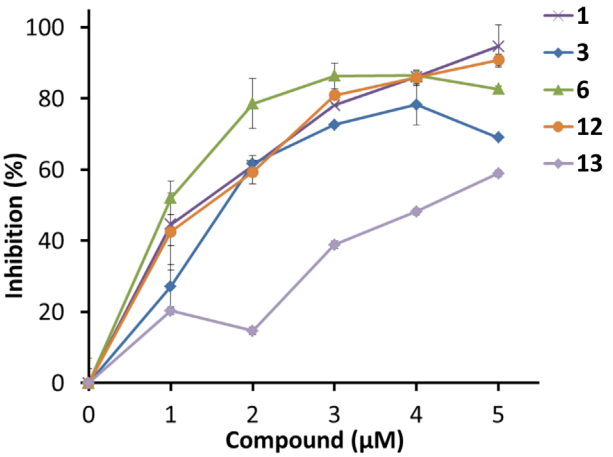

Figure 4. DHS inhibition potency of the derivatives selected for the HIV infection assay.

As expected, CNI-1493 (**1**) effectively inhibited HIV-1 replication in a dose-dependent manner beginning at a concentration of 0.5 μM. CNI-1493 analogue **3** exhibited a very similar inhibitory potential in this assay, showing efficient inhibition of the replication of HIV-1 BaL beginning at 0.5 μM as well (Fig. 5).

It is not clear why **6**, which proved to be active in the *in vitro* DHS-activity assay, showed no anti-HIV-1 activity in cell culture at similar concentrations as the other DHS inhibitors (Fig. 5). The aromatic CNI-1493 analogues, **12** and **13**, also inhibited HIV-1 replication albeit less potently, beginning at a concentration of 2 μM (Fig. 6). The result that none of the compounds exerted cellular toxicity in the tested concentration range (0.5–2 μM) is important to note (Figs. 5 and 6, lower panels). Since the cells are cultivated for at least 17 days in presence of CNI-1493 (**1**) and its analogues **3**, **6**, **12** and **13**, the maintained cellular metabolic activity including the measured redox-potential indicated a good cellular tolerance of the tested CNI-1493 derivatives.

Hydrolysis of CNI-1493

In the co-crystal structure of DHS and CNI-1493 (**1**), an aminoguanidine fragment (**15**) was observed in the active site. It was discussed above that this fragment **15** was inactive in the DHS assay (Fig. 3). However, this fragment may be formed by hydrolysis of **1** in the crystallisation buffer at longer periods of time. For a correct interpretation of the *in vitro* assays reported herein, it was required to prove that **1** and thus the new analogues **2**–**14** were stable under the conditions used in the assays. The hydrolysis of CNI-1493 using the conditions summarised in Table 1 was monitored by means of HPLC. 3′-Azidothymidine (AZT) was used as an internal standard. The UV-absorption spectrum of **1** showed an intense absorption at 264 nm.

Conditions 3–5 represent the media used in HIV-inhibition assays (3), crystallisation buffer experiments (4) and the DHS-inhibition assay (5), respectively. PBS buffer was used as an additional buffer. In acidic and slightly acidic media (pH 1.9–6.8), no hydrolysis of CNI-1493 (**1**) was observed for at least 5 days. However, under neutral as well as higher pH values, successive hydrolysis of **1** was detected (conditions 1, 4, 5, 10–13; Table 1).

In general, all observed hydrolysis products were more lipophilic resulting in a shift to higher retention times on the RP-18 column. Conditions 1 and 2 resulted in the same decomposition products independent of the temperature. However, **1** seemed to be more stable in DMSO alone than in DMSO/water as concluded from a longer half-life of about

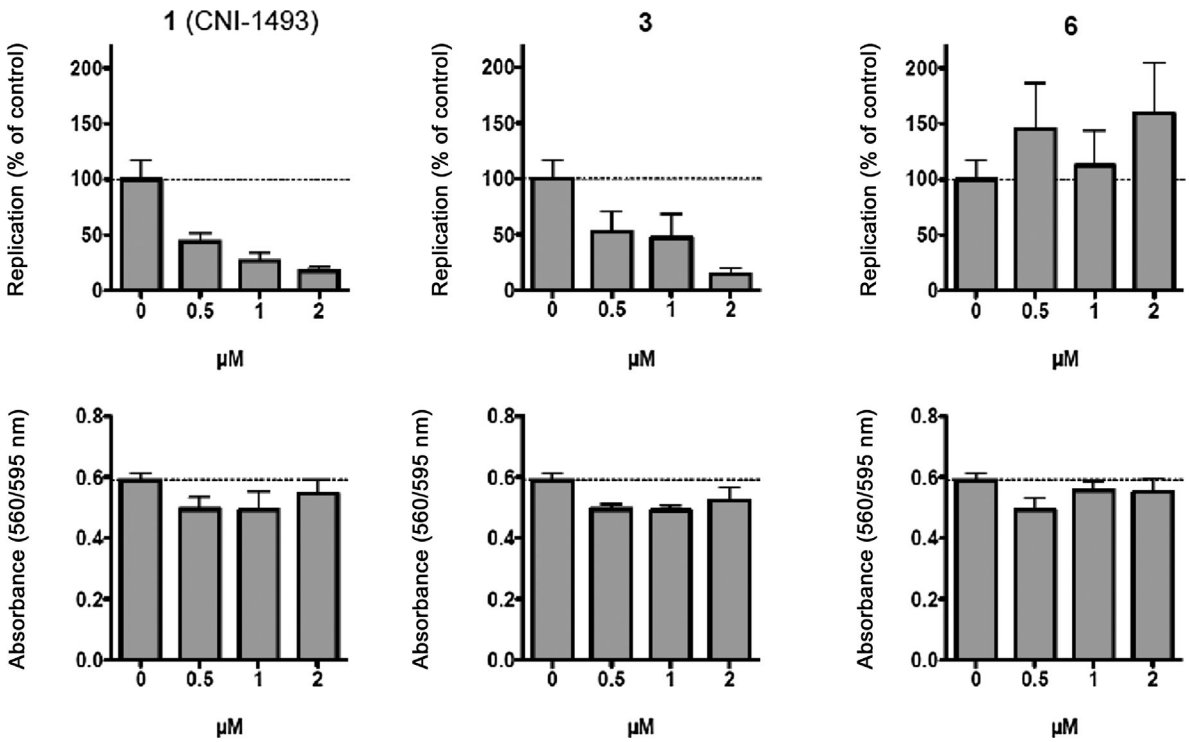

Figure 5. Anti-retroviral activity and cytotoxicity of the aliphatic CNI-1493 derivatives **3** and **6**. Mean values of at least six independent infections are shown. Upper panels show the percentage of virus replication as compared with replication in solvent control (DMSO)-cultures, which is arbitrarily set to 100% and depicted as a dotted line. AlamarBlue assays from the same cultures are shown in the lower panels.

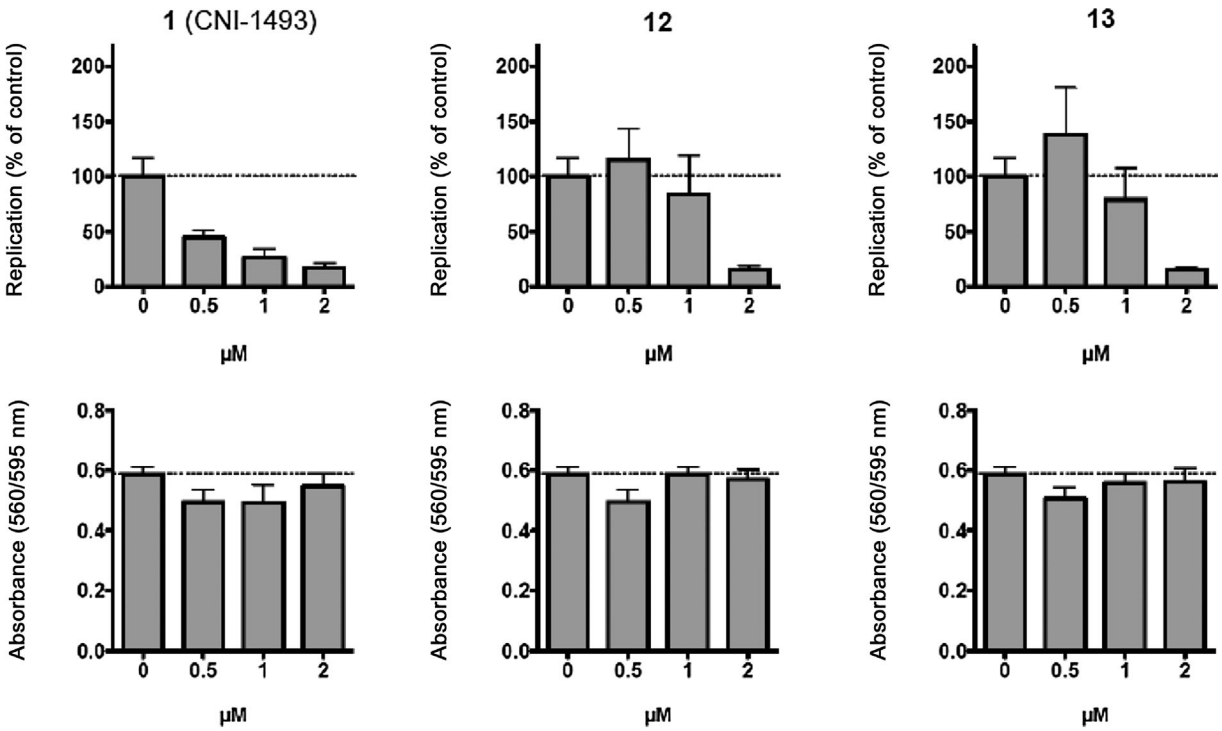

Figure 6. Antiretroviral activity and toxicity of the aromatic CNI-1493 derivatives **12** and **13**. Mean values of at least six independent infections are shown. Upper panels show the percentage of virus replication as compared with replication in solvent control (DMSO)-cultures, which is arbitrarily set to 100% and depicted as a dotted line. AlamarBlue assays from the same cultures are shown in the lower panels.

140 h compared to 87 h, respectively. In more basic buffers (pH >7.5), the hydrolysis products formed were found to be identical with those detected in H_2O (pH 7.0) and in DMSO. However, the hydrolysis in basic PBS buffer was significantly faster (half-live about 45 h) than in water (87 h). The hydrolysis of **1** in glycine buffer was analysed by mass spectrometry as an example for the identification of the hydrolysis products.

Two hydrolysis products could be identified via LC-MS as the monoketone ($t_R = 8.85$ min) and the diketone ($t_R = 10.35$ min) (Supporting Information Figs. S1 and S2). The third hydrolysis peak ($t_R = 12.65$ min) was not assigned by LC-MS, but is assumed to be the triketone. Due to the MS analysis, it could not be determined whether the second imine bond is cleaved at the same side as the first one or at the second head group.

Table 1. Summary of the conditions used in the hydrolysis studies.

Condition	Buffer	pH Value	Condition	Buffer	pH Value
1	DMSO	–	8	PBS[d]	6.0
2	Water	7.0	9	PBS[d]	6.8
3	RPMI-1640[a]	7.2	10	PBS[d]	7.5
4	Tris[b]	8.5	11	PBS[d]	8.5
5	Glycine[c]	9.0	12	PBS[d]	9.0
6	PBS[d]	1.9	13	PBS[d]	11.0
7	PBS[d]	4.0			

[a] RPMI-1640/heat-inactivated FCS (10%), 37°C.
[b] 100 mM Tris, 63% 2-methyl-2,4-pentanediol, 3 mM NAD, rt.
[c] 300 mM glycine, 37°C.
[d] 50 mM phosphate buffer, 37°C.

The half-live of **1** in the glycine buffer was determined to about 139 h, which was rather long regarding the basic buffer (condition 5, Table 1). Surprisingly, the hydrolysis in the crystallisation buffer (condition 4, Table 1) resulted in a fast decomposition of **1** with a half-live of only 22 h, which perfectly explains the appearance of the fragment in the DHS active site in the X-ray crystal structure analysis. In RPMI-1640, cell media CNI-1493 was found to be stable at 37°C for at least 4 days. All results indicated a successive hydrolysis of the imine bonds to the corresponding ketones under neutral and basic buffer conditions. A cleavage of the amide bond in the backbone was not observed, because no formation of the arylamine **14** was detected. Due to these results and the fact, that the CNI-1493 derivatives are modified in the diamide linker moiety, they should display comparable hydrolysis properties as obtained for compound **1**.

In silico docking studies

In a recent co-crystal structure [23], CNI-1493 (**1**) was found to bind to DHS at the surface of the protein, next to the entry to the binding site in a sandwich-like conformation. To investigate this binding site in more detail, a number of CNI-1493 analogues **2**–**14** were studied by computational means in order to find out if the CNI-1493 analogues reported herein were able to adopt a similar conformation at a low calculated potential energy. Therefore, the conformation adopted by CNI-1493 in the co-crystal structure was energy minimised using the MMFFx94 force field within MOE [27]. The aliphatic residue of the linker in CNI-1493 (**1**) has a length of eight methylene groups. The length of the linker was modified in the range of two to twelve methylene groups. In addition, the oxalyl group was studied as a linker (Fig. 2). Afterwards, energetically optimised conformations of these modifications of CNI-1493 were generated using the MMFF94x force field. Root-mean-square deviations (RMSD) were calculated with YASARA [28]. To calculate the RMSD, hydrogen atoms were neglected and structures were aligned and superposed allowing flipping of symmetrical groups. These minimised structures were superposed to the sandwich-like conformation of CNI-1493 as found in the co-crystal structure of the DHS/CNI-1493 complex (Fig. 7).

Although the optimal conformations of the CNI-1493 modifications slowly change with increasing length of the linker, the sandwich-like conformation becomes unlikely for shorter or rigid linkers. Therefore, the observed inhibitory activity of the CNI-1493 analogues **2**–**4**, **8**, **9**, **12** and **13** point to a binding mode different to the observed sandwich-like conformation, whereas **5**–**7**, **10** and **11** can adopt a conformation similar to the sandwich-like form.

MD simulations

In order to evaluate the stability of the CNI-1493 binding mode observed in the DHS:CNI-1493 complex and to investigate why the truncated version **14** is unable to block the DHS/eIF-5A interaction, comparative molecular dynamics (MD) simulations of DHS in complex with **1** as well as **14**

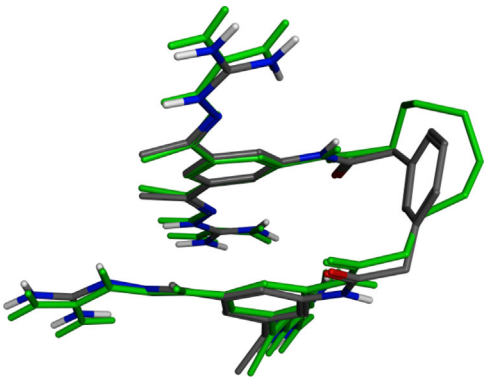

Figure 7. Superpositioning of minimised structures of CNI-1493 (**1**) (green) and **11** (carbon atoms in grey, nitrogen atoms in blue, oxygen atoms in red and hydrogen atoms in white) with an RMSD of 0.18 Å.

were performed (Supporting Information Fig. S3). X-ray crystal data of DHS complexed with CNI-1493 revealed the ligand to bind next to the entry to the spermidine pocket in a sandwich-like conformation. The guanidinium group of the inner CNI-1493 head group (directly bound to DHS) forms π–π interactions with the phenylalanine side chain of Phe247 and may interact with Glu180. The phenyl ring of the inner CNI-1493 half forms π–π stacking interactions with the phenyl ring of the outer half. This part of the molecule also forms two salt bridges between one of its guanidinium moieties and Glu180. At first, the stability of the reported DHS/CNI-1493 interactions was evaluated with an MD simulation using the GROMACS software. As ring orientations are difficult to compute in GROMACS, interactions between **1** and Phe247 were monitored indirectly by calculating the number of van-der-Waals (vdW) interactions between both moieties.

The guanidinium group of the inner CNI-1493 half extensively interacts with Phe247 (Supporting Information Fig. S3A). On average, 11.1 vdW contacts between atoms of the guanidinium moiety and the aromatic side chain were measured. Compared to the crystal structure, we observed significantly more vdW interactions (on average 5.15) between the inner half's phenyl ring and Phe247. In contrast to **1**, **14** revealed much less stable contacts between the guanidinium moiety and Phe247 (Supporting Information Fig. S3B). Only in a single simulation the molecule stably interacted with the phenyl ring throughout the course of the simulations. Also, interactions between the aromatic group of the ligand and Phe247 are marginal. Moreover, we have not found evidences for cation–π interactions. On average, only a single vdW contact was observed. In simulations of the DHS tetramer with bound CNI-1493, the salt bridge between the ligand and Glu180 is stable in most simulations (average bond $>$0.5), although with large fluctuations (Supporting Information Fig. S3C). In addition, a salt bridge between **1** and Asp243, located in the tunnel that connects the spermidine pocket

with the protein surface, is observed (Supporting Information Fig. S3E). In comparison with **1**, simulations including the truncated molecule **14** did not reveal any significant interaction with Glu180 (Supporting Information Fig. S3D) and contacts with Asp243 were found only in a single simulation run (Supporting Information Fig. S3F). Compared to the extensive interactions between the guanidinium group and Phe247, the aromatic rings of **1** interact much less with each other (Supporting Information Fig. S3G). The number of vdW contacts is even lower than the interactions between the aromatic ring of the inner CNI-1493 head group and Phe247 (on average 3.2 vdW contacts). The significantly less pronounced interactions are due to reorientation of the outer half of the ligand. The RMSD-plots of CNI-1493 heavy atoms clearly indicate the conformational change in four of the six molecules simulated (Supporting Information Fig. S3H). Only two CNI-1493 molecules revealed the stacked-like conformation observed in the X-ray crystal structure. In those cases, an intramolecular hydrogen bond either formed between a guanidinium moiety of one CNI-1493 half and the carbonyl group of the second half or both amide moieties was observed that restricts the conformational flexibility (Supporting Information Fig. S3H).

The results confirm several protein–ligand interactions observed between **1** and DHS in the X-ray crystal structure. Moreover, an additional contact with an amino acid of the tunnel that connects the spermidine pocket with the solvent could be detected. In contrast to X-ray crystal data, the simulations suggest that the stacked conformation of **1** as observed in the X-ray crystal structure is not very stable. Only in few simulations the aromatic rings of both head groups were found to interact with each other. The simulations suggested that **14** will not stably bind to DHS as none of the interactions formed between DHS and **1** were present in the DHS/**14** complex. Comparing both simulations, the head group alone seems to be not sufficient for inhibiting the interaction of eIF-5A and DHS. The linker as well as the second head group needs to establish additional contacts with DHS and thus stabilise the interactions of the inner head group with Glu180, Asp243 and Phe247.

Conclusion

For closer insights into the structural factors influencing the antiviral activity and the binding mode of CNI-1493, several analogues of **1** were synthesised and analysed regarding their inhibitory potency against DHS *in vitro*. It was shown that the truncated derivative **14** and the aminoguanidine fragment **15** were found to be inactive. Most of the other analogues, containing different linkers between the head groups, showed dose-dependent activity against DHS. It can be concluded that two head groups linked at least by an oxaloyl-moiety are necessary for an inhibitory effect of these CNI-1493 derivatives. Interestingly, the rigid derivatives **12** and **13** were also found to inhibit the DHS even though they are unable to adopt the conformation of **1** as observed in the co-crystal structure with DHS. This may point to an alternative binding mode of these compounds to the enzyme. This is supported by the fact that **11** turned out to only marginally inhibit the DHS, even though it can perfectly adapt the sandwich-like shape as calculated by minimised energy simulations. MD simulations showed that the stacked conformation of **1** in the crystal seems to be not very stable in solution, supporting the experimentally measured activity of the rigid derivatives. Moreover, the simulations provide structural evidence for the inability of **14** to inhibit DHS. None of the new derivatives tested in cell culture against HIV-1 showed cytotoxicity in concentrations up to 2 μM. **3**, **12** and **13** proved to inhibit the HIV-1 replication efficiently in a dose-dependent manner. In addition to the results of the enzymatic assay, these results support the hypothesis of a different binding mode of these rigid derivatives. The chemical stability was analysed using **1** as an example and showed successive cleavage of the imine bonds under basic conditions, whereas acidic conditions did not affect the stability of **1**. This is consistent with the observation that the aminoguanidine fragment **15** was found in the spermidine pocket of the DHS under basic conditions. Experiments to co-crystallise the CNI-1493 derivatives reported herein with DHS and tests against cART resistant virus strains are currently ongoing.

Experimental

Chemistry

General

All air- or water-sensitive reactions were performed in flame-dried glassware under a nitrogen atmosphere. Commercially available solvents and reagents were used without further purification with the following exceptions: dichloromethane (CH_2Cl_2) was distilled from calcium hydride and stored over activated molecular sieve. Tetrahydrofurane (THF) was dried over potassium/benzophenone, distilled under nitrogen and stored over activated molecular sieve. Petroleum ether 50–70, EtOAc, CH_2Cl_2 and CH_3OH employed in chromatography were distilled before use. For column chromatography, silica gel 60, 230–400 mesh was used. Pre-coated aluminium plates 60 F_{254} with 0.2 mm layer of silica gel containing a fluorescence indicator were used for thin layer chromatography (TLC). NMR spectra were recorded on 400 or 500 MHz spectrometers (Bruker AMX 400, Bruker AV 400 or Bruker DRX 500). All ^{1}H and ^{13}C NMR chemical shifts (δ) are quoted in parts per million (ppm) and were calibrated on solvent signals. High resolution mass spectra were obtained with a VG Analytical VG/70-250F spectrometer (FAB, matrix was *m*-nitrobenzyl alcohol). HR-ESI mass spectra were obtained with an Agilent Technologies ESI-TOF 6224 spectrometer. IR spectra were acquired using a Bruker Alpha-P IR spectrometer within 400–4000 cm^{-1} working in the attenuated total reflection (ATR) mode. Analytical HPLC was carried out on a VWR-Hitachi LaChromElite HPLC system consisting of a VWR-Hitachi L-2130 pump, L-2200 autosampler

and a diode array detector L-2455. The column used was a Nucleodur® C18 Gravity (EC, 125/4.6, 5 μm, Macherey–Nagel). Elution was performed using a 100 mM ammonium formate buffer (pH 3.0)/acetonitrile (Sigma–Aldrich, HPLC grade) eluent: 5–44% CH_3CN (0–12 min), flow rate 1.3 mL/min and UV detection at 264 nm. The purity of tested CNI-1493 derivatives **1–14** was checked by means of HPLC and was in all cases ≥95%. LC-MS analysis was carried out with the same solvents noted above using an Agilent Technologies Extend-C18 (1.8 μm, 2.1 mm × 50 mm) column on an Agilent Technologies 1200 series HPLC equipped with an Agilent Technologies ESI-TOF 6224 spectrometer.

*General procedure for the preparation of the aminoguanidine compounds **1–14***

The corresponding diamide **20–33** and 5 eq. aminoguanidine hydrochloride were dissolved in 3–5 mL ethanol/water (9:1) and 2 drops of conc. hydrochloric acid were added. After that, the reaction mixture was refluxed for 3 h. The pure product precipitated as its hydrochloride after storing the reaction mixture at −26°C. The precipitated product was collected by filtration, washed with 10 mL −26°C cold ethanol and 2 mL cold water and dried *in vacuo*. (See also the Supporting Information for the InChI codes.)

*N,N′-Bis[3,5-bis[1(aminoiminomethyl)-hydrazoethyl]-phenyl]-decane diamide tetrahydrochloride **1***

The reaction was performed according to the general procedure using **25** (533 mg, 1.02 mmol), amino guanidine hydrochloride (579 mg, 5.24 mmol) and 5 mL ethanol/water (9:1) yielding a colourless solid (696 mg, 0.781 mmol, 76%). ^{1}H NMR (400 MHz, DMSO-d_6): $\delta = 11.23$ (brs, 4H, guanidino-NH), 10.17 (s, 2H, amide-NH), 8.12 (d, $J = 1.6$ Hz, 4H, H-2/-6), 8.04 (t, $J = 1.6$ Hz, 2H, H-4), 7.81 (brs, 12H, guanidino-N_2H_3), 2.37 (s, 12H, CH_3), 2.33 (t, $J = 7.4$ Hz, 4H, H-a), 1.62–1.59 (m, 4H, H-b), 1.33–1.30 (m, 8H, H-c/-d) ppm. ^{13}C NMR (101 MHz, DMSO-d_6): $\delta = 171.6$ (amide-C), 156.0 (guanidino-C), 151.8 (imino-C), 139.4 (C-1), 137.4 (C-3/-5), 118.9 (C-2/-4/-6), 36.4 (C-a), 28.7 (C-c/-d), 25.0 (C-b), 15.2 (CH_3) ppm. IR (neat) $\tilde{\nu} = 2987$, 2901, 1451, 1075 and 892 cm^{-1}. HRMS (FAB) *m/z* = calcd. 745.4598 $[M+H]^+$, found 745.4614 $[M+H]^+$.

*N,N′-Bis[3,5-bis[1(aminoiminomethyl)-hydrazoethyl]-phenyl]ethyl diamide tetrahydrochloride **2***

The reaction was performed according to the general procedure using **21** (91 mg, 0.22 mmol), amino guanidine hydrochloride (125 mg, 1.13 mmol) and 5 mL ethanol/water (9:1) yielding a colourless solid (94 mg, 0.12 mmol, 55%). ^{1}H NMR (500 MHz, DMSO-d_6): $\delta = 11.31$ (brs, 4H, guanidino-NH), 10.81 (s, 2H, amide-NH), 8.43 (d, $J = 1.5$ Hz, 4H, H-2/-6), 8.17 (s, 2H, H-4), 7.82 (brs, 12H, guanidino-N_2H_3), 2.41 (s, 12H, CH_3) ppm. ^{13}C NMR (125 MHz, DMSO-d_6): $\delta = 158.3$ (amide-C), 156.1 (guanidino-C), 151.3 (imino-C), 137.8 (C-3/-5), 137.7 (C-1), 120.9 (C-4), 119.8 (C-2/-6), 14.7 (CH_3) ppm. IR (neat) $\tilde{\nu} = 3305$, 3151, 1669, 1588 and 1348 cm^{-1}. HRMS (ESI$^+$) *m/z* = calcd. 633.3341 $[M+H]^+$, found 633.3347 $[M+H]^+$.

*N,N′-Bis[3,5-bis[1(aminoiminomethyl)-hydrazoethyl]-phenyl]-butane diamide tetrahydrochloride **3***

The reaction was performed according to the general procedure using **22** (148 mg, 0.339 mmol), amino guanidine hydrochloride (192 mg, 1.73 mmol) and 3 mL ethanol/water (9:1) yielding a pale grey solid (259 mg, 0.322 mmol, 95%). ^{1}H NMR (400 MHz, DMSO-d_6): $\delta = 11.28$ (brs, 4H, guanidino-NH), 10.31 (s, 2H, amide-NH), 8.13 (s, 4H, H-2/-6), 8.04 (s, 2H, H-4), 7.82 (brs, 12H, guanidino-N_2H_3), 2.72 (s, 4H, butyl-H), 2.38 (s, 12H, CH_3) ppm. ^{13}C NMR (101 MHz, DMSO-d_6): $\delta = 170.1$ (amide-C), 156.1 (guanidino-C), 151.8 (imino-C), 139.5 (C-1), 137.7 (C-3/-5), 118.8 (C-4), 118.7 (C-2/-6), 56.0 (butyl-C), 15.2 (CH_3) ppm. IR (neat) $\tilde{\nu} = 3236$, 3075, 1667, 1590 and 1355 cm^{-1}. HRMS (FAB) *m/z* = calcd. 661.3659 $[M+H]^+$, found 661.3660 $[M+H]^+$.

*N,N′-Bis[3,5-bis[1(aminoiminomethyl)-hydrazoethyl]-phenyl]-hexane diamide tetrahydrochloride **4***

The reaction was performed according to the general procedure using **23** (137 mg, 0.294 mmol), amino guanidine hydrochloride (151 mg, 1.36 mmol) and 3 mL ethanol/water (9:1) yielding a colourless solid (121 mg, 0.145 mmol, 49%). ^{1}H NMR (400 MHz, DMSO-d_6): $\delta = 11.33$ (brs, 4H, guanidino-NH), 10.30 (s, 2H, amide-NH), 8.17 (s, 4H, H-2/-6), 8.05 (s, 2H, H-4), 7.85 (brs, 12H, guanidino-N_2H_3), 2.41 (s, 4H, H-a), 2.39 (s, 12H, CH_3), 1.67 (s, 4H, H-b) ppm. ^{13}C NMR (101 MHz, DMSO-d_6): $\delta = 171.3$ (amide-C), 156.0 (guanidino-C), 151.6 (imino-C), 139.4 (C-1), 137.5 (C-3/-5), 119.4 (C-4), 118.8 (C-2/-6), 36.3 (C-a), 24.6 (C-b), 15.1 (CH_3) ppm. IR (neat) $\tilde{\nu} = 3107$, 1666, 1593 and 1353 cm^{-1}. HRMS (FAB) *m/z* = calcd. 689.3973 $[M+H]^+$, found 689.3985 $[M+H]^+$.

*N,N′-Bis[3,5-bis[1(aminoiminomethyl)-hydrazoethyl]-phenyl]-octane diamide tetrahydrochloride **5***

The reaction was performed according to the general procedure using **24** (201 mg, 0.408 mmol), amino guanidine hydrochloride (221 mg, 2.00 mmol) and 3 mL ethanol/water (9:1) yielding a colourless solid (203 mg, 0.238 mmol, 58%). ^{1}H NMR (400 MHz, DMSO-d_6): $\delta = 11.32$ (brs, 4H, guanidino-NH), 10.22 (s, 2H, amide-NH), 8.15 (d, $J = 1.4$ Hz, 4H, H-2/-6), 8.04 (s, 2H, H-4), 7.85 (brs, 12H, guanidino-N_2H_3), 2.38 (s, 12H, CH_3), 2.36–2.28 (m, 4H, H-a), 1.70–1.58 (m, 4H, H-b), 1.35 (s, 4H, H-c) ppm. ^{13}C NMR (101 MHz, DMSO-d_6): $\delta = 171.4$ (amide-C), 156.0 (guanidino-C), 151.6 (imino-C), 139.4 (C-1), 137.4 (C-3/-5), 119.4 (C-4), 118.7 (C-2/-6), 36.2 (C-a), 28.3 (C-c), 24.7 (C-b), 15.1 (CH_3) ppm. IR (neat) $\tilde{\nu} = 3338$, 3167, 1678, 1587 and 1355 cm^{-1}. HRMS (FAB) *m/z* = calcd. 717.4286 $[M+H]^+$, found 717.4304 $[M+H]^+$.

*N,N′-Bis[3,5-bis[1(aminoiminomethyl)-hydrazoethyl]-phenyl]dodecane diamide tetrahydrochloride **6***

The reaction was performed according to the general procedure using **26** (158 mg, 0.289 mmol), amino guanidine hydrochloride (175 mg, 1.59 mmol) and 3 mL ethanol/water (9:1) yielding a colourless solid (181 mg, 0.197 mmol, 68%). ^{1}H NMR (400 MHz, DMSO-d_6): $\delta = 11.24$ (brs, 4H, guanidino-NH),

10.16 (s, 2H, amide-NH), 8.12 (d, $J = 1.5$ Hz, 4H, H-2/-6), 8.04 (t, $J = 1.5$ Hz, 2H, H-4), 7.81 (brs, 12H, guanidino-N_2H_3), 2.37 (s, 12H, CH_3), 2.33 (t, $J = 7.5$ Hz, 4H, H-a), 1.62–1.57 (m, 4H, H-b), 1.28 (s, 12H, H-c/-d/-e) ppm. ^{13}C NMR (101 MHz, DMSO-d_6): $\delta = 171.5$ (amide-C), 156.0 (guanidino-C), 151.6 (imino-C), 139.4 (C-1), 137.5 (C-3/-5), 118.8 (C-4), 118.7 (C-2/-6), 36.2 (C-a), 28.8, 28.7, 28.6 (C-c/-d/-e), 24.9 (C-b), 15.1 (CH_3) ppm. IR (neat) $\tilde{\nu} = 3130$, 1659, 1587 and 1355 cm^{-1}. HRMS (FAB) *m/z* = calcd. 773.4912 $[M+H]^+$, found 773.4938 $[M+H]^+$.

N,N′-Bis[3,5-bis[1(aminoiminomethyl)-hydrazoethyl]-phenyl]tetradecane diamide tetrahydrochloride ***7***

The reaction was performed according to the general procedure using **27** (136 mg, 0.236 mmol), amino guanidine hydrochloride (130 mg, 1.20 mmol) and 5 mL ethanol/water (9:1) yielding a colourless solid (80 mg, 84 μmol, 36%). ^{1}H NMR (400 MHz, DMSO-d_6): $\delta = 11.24$ (brs, 4H, guanidino-NH), 10.15 (s, 2H, amide-NH), 8.12 (d, $J = 1.2$ Hz, 4H, H-2/-6), 8.04 (t, $J = 1.4$ Hz, 2H, H-4), 7.81 (brs, 12H, guanidino-N_2H_3), 2.37 (s, 12H, CH_3), 2.33 (t, $J = 7.6$ Hz, 4H, H-a), 1.59 (q, $J = 6.7$ Hz, 4H, H-b), 1.32–1.23 (m, 16H, H-c/-d/-e/-f) ppm. ^{13}C NMR (101 MHz, DMSO-d_6): $\delta = 171.6$ (amide-C), 156.0 (guanidino-C), 151.8 (imino-C), 139.5 (C-1), 137.6 (C-3/-5), 118.9 (C-4), 118.4 (C-2/-6), 36.4 (C-a), 29.0, 28.9, 28.7 (C-c/-d/-e/-f), 25.0 (C-b), 15.2 (CH_3) ppm. IR (neat) $\tilde{\nu} = 3139$, 1921, 1670, 1586, 1443, 1273 and 1123 cm^{-1}. MS (FAB) *m/z* = calcd. 801.5 $[M+H]^+$, found 801.5 $[M+H]^+$.

N,N′-Bis[3,5-bis[1(aminoiminomethyl)-hydrazoethyl]-phenyl] (cis/trans)-1,4-cyclohexyl diamide tetrahydrochloride ***8***

The reaction was performed according to the general procedure using **28** (200 mg, 0.410 mmol), amino guanidine hydrochloride (225 mg, 2.04 mmol) and 5 mL ethanol/water (9:1) yielding a pale brown solid (70 mg, 90 μmol, 24%). ^{1}H NMR (400 MHz, DMSO-d_6): $\delta = 11.17$ (brs, 4H, guanidino-NH), 10.06 (s, 2H, amide-NH), 8.16–8.14 (m, 4H, H-2/-6), 8.05 (brs, 2H, H-4), 7.78 (brs, 12H, guanidino-N_2H_3), 2.62–2.55 (m, 2H, cyclohexyl-H-a), 2.37 (s, 12H, CH_3), 2.01–1.95 (m, 4H, cyclohexyl-H-b), 1.68–1.50 (m, 4H, cyclohexyl-H-b) ppm. ^{13}C NMR (101 MHz, DMSO-d_6): $\delta = 174.2$ (amide-C), 156.0 (guanidino-C), 151.8 (imino-C), 139.7 (C-1), 137.6 (C-3/-5), 118.9 (C-4), 118.7 (C-2/-6), 41.4 (cyclohexyl-C-a), 26.5 (cyclohexyl-C-b), 15.2 (CH_3) ppm. IR (neat) $\tilde{\nu} = 3138$, 1667, 1589, 1443, 1138 and 862 cm^{-1}. HRMS (FAB) *m/z* = calcd. 715.4129 $[M+H]^+$, found 715.4143 $[M+H]^+$.

N,N′-Bis[3,5-bis[1(aminoiminomethyl)-hydrazoethyl]-phenyl]-2-butene diamide tetrahydrochloride ***9***

The reaction was performed according to the general procedure using **29** (150 mg, 0.350 mmol), amino guanidine hydrochloride (191 mg, 1.70 mmol) and 5 mL ethanol/water (9:1) yielding a pale grey solid (156 mg, 0.194 mmol, 55%). ^{1}H NMR (400 MHz, DMSO-d_6): $\delta = 11.26$ (brs, 4H, guanidino-NH), 10.93 (s, 2H, amide-NH), 8.23 (s, 4H, H-2/-6), 8.11 (s, 2H, H-4), 7.82 (brs, 12H, guanidino-N_2H_3), 7.26 (s, 2H, H-a), 2.41 (s, 12H, CH_3) ppm. ^{13}C NMR (101 MHz, DMSO-d_6): $\delta = 162.6$ (amide-C), 156.1 (guanidino-C), 151.7 (imino-C), 139.0 (C-1), 137.8 (C-3/-5), 134.1 (C-a), 120.2 (C-4), 119.2 (C-2/-6), 15.1 (CH_3) ppm. IR (neat) $\tilde{\nu} = 2987$, 2971, 2900, 1394, 1250 and 1065 cm^{-1}. HRMS (FAB) *m/z* = calcd. 659.3503 $[M+H]^+$, found 659.3505 $[M+H]^+$.

N,N′-Bis[3,5-bis[1(aminoiminomethyl)-hydrazoethyl]-phenyl]-1,4-phenylacetyl diamide tetrahydrochloride ***10***

The reaction was performed according to the general procedure using **30** (120 mg, 0.230 mmol), amino guanidine hydrochloride (129 mg, 1.20 mmol) and 5 mL ethanol/water (9:1) yielding a colourless solid (171 mg, 0.194 mmol, 84%). ^{1}H NMR (400 MHz, DMSO-d_6): $\delta = 11.20$ (brs, 4H, guanidino-NH), 10.53 (s, 2H, amide-NH), 8.13 (s, 2H, H-4), 8.04 (s, 2H, H-2/-6), 7.79 (brs, 12H, guanidino-N_2H_3), 7.32 (s, 4H, H-2′), 3.66 (s, 4H, CH_2), 2.36 (s, 12H, CH_3) ppm. ^{13}C NMR (101 MHz, DMSO-d_6): $\delta = 169.6$ (amide-C), 156.0 (guanidino-C), 151.8 (imino-C), 139.4 (C-1), 137.6 (C-3/-5), 134.0 (C-1′), 129.1 (C-2′), 118.9 (C-2/-6), 118.6 (C-4), 42.6 (CH_2), 15.1 (CH_3) ppm. IR (neat) $\tilde{\nu} = 2987$, 2901, 1588, 1406, 1229, 1066 and 899 cm^{-1}. MS (ESI$^+$) *m/z* = calcd. 737.3967 $[M+H]^+$, found 737.3956 $[M+H]^+$.

N,N′-Bis[3,5-bis[1(aminoiminomethyl)-hydrazoethyl]-phenyl]-1,3-phenylacetyl diamide tetrahydrochloride ***11***

The reaction was performed according to the general procedure using **31** (120 mg, 0.230 mmol), amino guanidine hydrochloride (130 mg, 1.17 mmol) and 5 mL ethanol/water (9:1) yielding a colourless solid (81 mg, 92 μmol, 40%). ^{1}H NMR (400 MHz, DMSO-d_6): $\delta = 11.21$ (brs, 4H, guanidino-NH), 10.55 (s, 2H, amide-NH), 8.15 (s, 2H, H-4), 8.05 (s, 2H, H-2/-6), 7.80 (brs, 12H, guanidino-N_2H_3), 7.33 (s, 1H, H-2′), 7.31–7.25 (m, 3H, H-4′/-5′/-6′), 3.69 (s, 4H, CH_2), 2.36 (s, 12H, CH_3) ppm. ^{13}C NMR (101 MHz, DMSO-d_6): $\delta = 169.4$ (amide-C), 156.0 (guanidino-C), 151.8 (imino-C), 139.4 (C-1), 137.7 (C-3/-5), 135.7 (C-1′/-3′), 130.1 (C-2′), 128.3, 127.6 (C-4′/-5′/-6′), 119.3 (C-2/-6), 118.6 (C-4), 43.2 (CH_2), 15.2 (CH_3) ppm. IR (neat) $\tilde{\nu} = 3120$, 1667, 1584, 1440, 1354, 1127 and 874 cm^{-1}. HRMS (FAB) *m/z* = calcd. 737.3973 $[M+H]^+$, found 737.4009 $[M+H]^+$.

N,N′-Bis[3,5-bis[1(aminoiminomethyl)-hydrazoethyl]-phenyl]-1,4-benzene diamide tetrahydrochloride ***12***

The reaction was performed according to the general procedure using **32** (226 mg, 0.447 mmol), amino guanidine hydrochloride (263 mg, 2.38 mmol) and 5 mL ethanol/water (9:1) yielding a colourless solid (198 mg, 0.279 mmol, 60%). ^{1}H NMR (400 MHz, DMSO-d_6): $\delta = 11.35$ (brs, 4H, guanidino-NH), 10.71 (s, 2H, amide-NH), 8.42 (s, 4H, H-2/-6), 8.24 (s, 4H, H-b), 8.13 (s, 2H, H-4), 7.87 (brs, 12H, guanidino-N_2H_3), 2.43 (s, 12H, CH_3) ppm. ^{13}C NMR (101 MHz, DMSO-d_6): $\delta = 164.7$ (amide-C), 156.1 (guanidino-C), 151.6 (imino-C), 139.1 (C-1), 137.6 (C-3/-5), 137.1 (C-a), 127.9 (C-b), 120.7 (C-2/-6), 120.5 (C-4), 15.2 (CH_3) ppm. IR (neat) $\tilde{\nu} = 3340$, 3150, 1668 and 1357 cm^{-1}. HRMS (FAB) *m/z* = calcd. 709.3659 $[M+H]^+$, found 709.3671 $[M+H]^+$.

N,N′-Bis[3,5-bis[1(aminoiminomethyl)-hydrazoethyl]-phenyl]-1,3-benzene diamide tetrahydrochloride ***13***

The reaction was performed according to the general procedure using **33** (210 mg, 0.412 mmol), amino guanidine hydrochloride (228 mg, 2.06 mmol) and 5 mL ethanol/water (9:1) yielding a colourless solid (231 mg, 0.270 mmol, 66%). ^{1}H NMR (400 MHz, DMSO-d_6): $\delta = 11.31$ (brs, 4H, guanidino-NH), 10.91 (s, 2H, amide-NH), 9.05 (s, 1H, H-2′), 8.59 (s, 4H, H-2/-6), 8.25 (d, $J = 7.7$ Hz, 2H, H-4′/-6′), 8.13 (s, 2H, H-4), 7.86 (brs, 12H, guanidino-N_2H_3), 7.74 (t, $J = 7.7$ Hz, 1H, H-5′), 2.44 (s, 12H, CH_3) ppm. ^{13}C NMR (101 MHz, DMSO-d_6): $\delta = 164.7$ (amide-C), 156.1 (guanidino-C), 151.7 (imino-C), 139.4 (C-1), 137.6 (C-3/-5), 134.3 (C-1′/-3′), 130.9 (C-4′/-6′), 128.8 (C-5′), 126.0 (C-2′), 120.3 (C-4), 119.7 (C-2/-6), 15.1 (CH_3) ppm. IR (neat) $\tilde{\nu} = 2987$, 2900, 1406, 1250, 1066 and 892 cm^{-1}. HRMS (FAB) m/z = calcd. 709.3660 $[M+H]^+$, found 709.3680 $[M+H]^+$.

DHS activity assay

The deoxyhypusine synthase reaction was conducted in principle as described previously [29]. Briefly, the reaction mixture contained 5 μg eIF-5A precursor protein, 3 μg DHS and 2 μCi [^{3}H]-spermidine (32.4 Ci/mmol) in a total volume of 200 μL reaction buffer (300 mM glycine-NaOH, pH 9.0, 1 mM NAD^+, 1 mM DTT, 50 μg/mL BSA). In order to test a possible influence of the new inhibitors on DHS activity, the enzymatic reaction was performed in the presence of the indicated concentrations of the indicated CNI-1493 derivatives, or with CNI-1493 as a positive control or without compounds as a solvent or negative control, respectively. After 1 h at 37°C, the reaction was stopped by adding 200 μL of 20 mM spermidine in PBS and transferred onto a Millipore GSWPO2500 nitrocellulose membrane, which was previously blocked with 20 mM spermidine/PBS for 1 h. The reaction mixture was vacuum filtered followed by washing the membrane with 5 mL PBS. Finally, the membranes were air dried and the tritium signal was measured in a liquid scintillation counter.

Overexpression and purification of DHS and eIF-5A

The *Escherichia coli* strain BL21 (DE3) (Novagen) was employed for protein expression.

His-DHS purification

pTricHis-DHS clone was used for the preparation for recombinant DHS [19]. A 1 L culture of LB-ampicillin medium was inoculated with a 50 mL overnight culture of *E. coli* BL21 (DE3) transformed with pTricHis-DHS (preinoculum) and grown at 37°C until the optical density (OD) value at 600 nm reached 0.6–0.8 (~3 h). The Tre recombinase gene expression was induced by addition of 0.5 mM of IPTG, and was further grown for a period of 4 h at 37°C. Post incubation the bacteria were harvested by centrifugation (10 min, 5000*g*, 4°C) and stored at −80°C until further use. The cell pellet was resuspended in 30 mL lysis buffer (50 mM Tris pH 8, 300 mM NaCl and 30 mM imidazole) and lysed by sonication. The soluble fraction was separated by centrifugation at 12000 rpm for 15 min. About 1 mL bed volume of buffer-equilibrated Ni-NTA beads was added to the supernatant and incubated with gentle rocking in an end-to-end rotor at 4°C for 1 h. The beads were then packed in a column and washed with wash buffer (50 mM Tris pH 8, 300 mM NaCl and 30 mM imidazole), followed by second wash buffer (50 mM Tris pH 8, 300 mM NaCl and 50 mM imidazole). The protein was eluted in 50 mM Tris pH 8, 300 mM NaCl and 300 mM imidazole. The purified His-DHS protein was analysed on SDS-PAGE and was dialysed against 300 mM glycine NaOH, pH 9 and 10 % glycerol and stored at −20°C.

eIF-5A expression and purification

pGEX-eIF-5A clone was used to prepare eIF-5A protein as described in [19], with minor modifications. GST-eIF-5A overexpression was performed as described for DHS. IPTG-induced cell pellet was resuspended in 40 mL lysis buffer (10 mM PBS pH 7.4, 1 mM DTT, 5 mM EDTA, 2.6 mM $MnCl_2$, 26 mM $MgCl_2$) with 0.5 μg/mL DNAse and protease inhibitors (0.1 mM PMSF, 2 μg/mL leupeptin, 2 μg/mL aprotinin) and lysed by sonication. To the total lysate, 1% Triton X-100 was added (Triton X-100 to be diluted in 1× PBS and then used) and incubated at 4°C for 1 h on an end-to-end rotor. The soluble fraction was separated by centrifuging at 30000*g* for 15 min. To the supernatant, 1 mL bed volume of buffer-equilibrated GSH beads were added and incubated with gentle rocking in an end-to-end rotor at 4°C for 1–2 h. The beads are then washed with 100 mL of wash buffer (50 mL PBS pH 7.4, 1 mM DTT and 5 mM EDTA) and with 150 mL of second buffer (50 mM Tris pH 8, 200 mM NaCl and 5 mM EDTA). The protein was eluted in 50 mM Tris-HCl, 200 mM NaCl and 20 mM reduced glutathione (pH 8.0). The purified protein fractions were dialysed against the factor Xa cleavage buffer, 50 mM Tris-HCl, 100 mM NaCl and 1 mM $CaCl_2$. Factor Xa cleavage and final purification of eIF-5A were performed exactly as described in [19]. eIF-5A was dialysed in assay buffer (300 mM glycine/NaOH, pH 9) and stored at −20°C.

HIV-1 infection experiments

PM1-cells were preincubated for 8–10 days and splitted according to culture density in presence of the inhibitor candidates or DMSO as solvent control. Subsequently, the cells were infected with the macrophage-tropic (R5) HIV-1 strain BaL [30]. For infection, roughly 3×10^6 cells were resuspended in 500 μL culture medium without drugs and incubated at 37°C for 3 h with 3 ng of HIV-1 viral stock. After infection, cells were washed twice with PBS and further cultivated in presence of the inhibitor candidates or DMSO. At day 3 post infection, the culture medium was replaced and cells were split. At day 7 post infection, p24-levels in the supernatant were determined by enzyme-linked immunosorbent assay (Innogenetics NV). Cellular viability was tested in parallel utilizing AlamarBlue (AbD Serotec). At least six independent infections were carried out for each tested concentration. PM1 cells were maintained in RPMI (Invitrogen) containing

10% FCS (Biochrom AG), 100 units/mL penicillin and 100 mg/mL streptomycin (Invitrogen). PM1 cells and the HIV-1 isolate BaL were obtained from the NIH AIDS Research and Reference Reagent Program.

MD simulations

Three-dimensional coordinates of the DHS tetramer in complex with two CNI-1493 molecules were taken from the unpublished crystal structure [23]. The protein was placed in a box with an edge length of 7.90 nm × 9.45 nm × 11.97 nm. Protonation states of all amino acid residues were adjusted according to the pK_a values in a medium of pH 7.4. Water molecules were represented using the SPC model [31]. In order to ensure neutrality of the system and to mimic a physiological NaCl solution, 77 Na^+ and 49 Cl^- ions were added to the systems.

Full-length CNI-1493, its truncated version and NAD were parameterised manually according to the GROMOS-96 topology and tested for reliability separately in a small water box (data not shown). Atomic point charges were calculated using the MMFF94x force field [30] within MOE [27]. All simulations were performed using GROMACS version 3.3.3 (parameter set 43a1) [32]. The resulting systems were minimised in a three-step procedure. Initially, positions of hydrogen atoms were optimised using 100 steps conjugate gradients with fixed heavy atoms. Subsequently, the whole system was minimised using two minimization procedures with 1000 steps steepest descents and conjugate gradients, respectively [33]. In order to minimise edge effects periodic boundary conditions were employed. The particle-mesh Ewald method was applied to accurately determine the long-range electrostatic interactions [34, 35]. VdW interactions were considered by applying a cutoff of 14 Å. The timestep for the simulations was set to 2 fs. The systems were gradually heated from 0 to 298 K using a simulated annealing protocol followed by an equilibration period of 5 ns. To keep the systems at constant temperature, a Berendsen thermostat was applied using a coupling time of 0.1 ps [36]. Constant pressure was maintained by coupling to an external bath with a reference value of 10^5 Pa, a coupling time of 1.0 ps and an isothermal compressibility of 4.5×10^{-10} Pa^{-1}. Bonds between heavy atoms and corresponding hydrogen atoms were constrained to their equilibrium bond lengths using the SHAKE algorithm [37]. Subsequent production runs of 50 ns length were performed using a Nose Hoover heat bath (coupling time 0.5 ps) and Parrinello–Rahman pressure coupling with a coupling time of 5.0 ps [38–41]. For each system three independent simulations were performed. Representative frames were obtained by clustering the trajectories over backbone atoms [42]. VdW contacts are defined as heavy atom distances $\leq$4.0 Å. Hydrogen bonds are defined by a donor–acceptor cutoff distance of $\leq$3.5 Å and a cutoff-angle of $\leq$30°. Figures were prepared using VMD and POV-ray [43, 44].

The authors are grateful to the Federal Ministry of Education and Research (BMBF) for financial support under grant 01 GU 0715–0718 'Combating drug resistance in CML and HIV-1 Infection'. We also thank Silke Kummer for excellent technical assistance and the other research groups collaborating in this project: Prof. Dr. T. Brümmendorf (Universitätsklinikum Aachen) and Dr. S. Balabanov (UniversitätsSpital Zürich).

The authors have declared no conflict of interest.

References

[1] M. H. Park, *J. Biochem*. **2006**, *139*, 161–169.
[2] E. C. Wolff, K. R. Kang, Y. S. Kim, M. H. Park, *Amino Acids* **2007**, *33*, 341–350.
[3] W. M. Kemper, K. W. Berry, W. C. Merrick, *J. Biol. Chem*. **1976**, *251*, 5551–5557.
[4] R. Benne, M. L. Brown-Luedi, J. W. Hershey, *J. Biol. Chem*. **1978**, *253*, 3070–3077.
[5] P. Saini, D. E. Eyler, R. Green, T. E. Dever, *Nature* **2009**, *459*, 118–121.
[6] A. P. Gregio, V. P. Cano, J. S. Avaca, S. R. Valentini, C. F. Zanelli, *Biochem. Biophys. Res. Commun*. **2009**, *380*, 785–790.
[7] C. H. Li, T. Ohn, P. Ivanov, S. Tisdale, P. Anderson, *PLoS ONE* **2010**, *5*, 9942.
[8] R. D. Robbins, S. A. Tersey, T. Ogihara, D. Gupta, T. B. Farb, J. Ficorilli, K. Bokvist, B. Maier, R. G. Mirmira, *J. Biol. Chem*. **2010**, *285*, 39943–39952.
[9] M. Kruse, O. Rosorius, F. Kratzer, D. Bevec, C. Kuhnt, A. Steinkasserer, G. Schuler, J. Hauber, *J. Exp. Med*. **2000**, *191*, 1581–1590.
[10] J. Chemnitz, N. Turza, I. Hauber, A. Steinkasserer, J. Hauber, *Immunobiology* **2010**, *215*, 370–379.
[11] B. Maier, T. Ogihara, A. P. Trace, S. A. Tersey, R. D. Robbins, S. K. Chakrabarti, C. S. Nunemaker, N. D. Stull, C. A. Taylor, J. E. Thompson, R. S. Dondero, E. C. Lewis, C. A. Dinarello, J. L. Nadler, R. G. Mirmira, *J. Clin. Invest*. **2010**, *120*, 2156–2170.
[12] G. Lipowsky, F. R. Bischoff, P. Schwarzmaier, R. Kraft, S. Kostka, E. Hartmann, U. Kutay, D. Görlich, *EMBO J*. **2000**, *19*, 4362–4371.
[13] D. Bevec, H. Jaksche, M. Oft, T. Woehl, M. Himmelspach, A. Pacher, M. Schebesta, K. Koettnitz, M. Dobrovnik, *Science* **1996**, *271*, 1858–1860.
[14] W. Hofmann, B. Reichart, A. Ewald, E. Müller, I. Schmitt, R. H. Stauber, F. Lottspeich, B. M. Jockusch, U. Scheer, J. Hauber, M.-C. Dabauvallea, *J. Cell Biol*. **2001**, *152*, 895–910.
[15] I. Hauber, D. Bevec, J. Heukeshoven, F. Kraetzer, F. Horn, A. Choidas, T. Harrer, J. Hauber, *J. Clin. Invest*. **2005**, *115*, 76–85.
[16] R. A. Hart, J. N. Billaud, S. J. Choi, T. R. Phillips, *Virology* **2002**, *304*, 97–104.
[17] A. Kaiser, *Amino Acid* **2010**, *42*, 679–684.
[18] S. V. Sitaraman, M. Hoteit, A. T. Gewirtz, *Curr. Opin. Investig. Drug* **2003**, *4*, 1363–1368.
[19] M. N. Sommer, D. Bevec, B. Klebl, B. Flicke, K. Hoelscher, T. Freudenreich, I. Hauber, J. Hauber, H. Mett, *J. Biomol. Screen*. **2004**, *9*, 434–438.

[20] P. Ziegler, T. Chahoud, T. Wilhelm, N. Paellman, M. Braig, V. Wiehle, S. Ziegler, M. Schroeder, C. Meier, A. Kolodzik, M. Rarey, J. Panse, J. Hauber, S. Balabanov, T. H. Bruemmendorf, *Invest. New Drug* **2012**, *30*, 2274–2283.
[21] M. Woriedh, I. Hauber, A. L. Martinez-Rocha, C. Voigt, F. J. Maier, M. Schroeder, C. Meier, J. Hauber, W. Schaefer, *Mol. Plant Microbe Interact.* **2011**, *24*, 619–627.
[22] H. Wang, M. Zhang, M. Bianchi, B. Sherry, A. Sama, K. J. Tracey, *Proc. Natl. Acad. Sci. USA* **1998**, *95*, 14429–14434.
[23] R. Hilgenfeld, **2014**, *unpublished*.
[24] D. M. McKinnon, J. Y. Wong, *Can. J. Chem.* **1971**, *49*, 2018–2022.
[25] P. Ulrich, A. Crami, *J. Med. Chem.* **1984**, *27*, 35–40.
[26] M. Bianchi, P. Ulrich, O. Bloom, M. III Meistrell, G. A. Zimmerman, H. Schmidtmayerova, M. Bukrinsky, T. Donnelley, R. Bucala, B. Sherry, K. R. Manogue, A. J. Tortolani, A. Cerami, K. J. Tracey, *Mol. Med.* **1995**, *1*, 254–266.
[27] MOE, v 2010-10, Chemical Computing Group, http://www.chemcomp.com/software.htm.
[28] YASARA, version 8-10-13, http://www.yasara.org.
[29] D. Bevec, B. Kappel, H. Jaksche, R. Csonga, J. Hauber, H. Klier, A. Steinkasserer, *FEBS Lett.* **1996**, *378*, 195–198.
[30] S. Gartner, P. Markovits, D. M. Markovitz, M. H. Kaplan, R. C. Gallo, M. Popovic, *Science* **1986**, *233*, 215–219.
[31] H. J. C. Berendsen, J. P. M. Postma, W. F. van Gunsteren, J. Hermans, in *Intermolecular Forces*. (Ed.: B. Pullman), D. Reidel Publishing Company, Dordrecht **1981**, pp. 331–342.
[32] T. A. Halgren, *J. Comput. Chem.* **1996**, *17*, 490–519.
[33] D. van der Spoel, E. Lindahl, B. Hess, G. Groenhof, A. E. Mark, H. J. Berendsen, *J. Comput. Chem.* **2005**, *16*, 1701–1718.
[34] W. R. P. Scott, Hünenberger, I. G. Tironi, A. E. Mark, S. R. Billeter, J. Fennen, A. E. Torda, T. Huber, P. Krüger, W. F. van Gunsteren, *J. Phys. Chem. A* **1999**, *103*, 3596–3607.
[35] T. A. Darden, D. York, L. Pedersen, *J. Chem. Phys.* **1993**, *98*, 10089–10092.
[36] U. Essmann, L. Perera, M. L. Berkowitz, T. Darden, H. Lee, L. G. Pedersen, *J. Comp. Phys.* **1995**, *103*, 8577–8592.
[37] H. J. C. Berendsen, J. P. M. Postma, A. Dinola, J. R. Haak, *J. Chem. Phys.* **1984**, *81*, 3684–3690.
[38] J. P. Ryckaert, G. Ciccotti, H. J. C. Berendsen, *J. Comp. Phys.* **1977**, *23*, 327–341.
[39] W. G. Hoover, *Phys. Rev. A.* **1985**, *31*, 1695–1697.
[40] A. Nosé, *Mol. Phys.* **1984**, *52*, 255–268.
[41] M. Parrinello, A. Rahman, *J. Appl. Phys.* **1981**, *52*, 7182–7190.
[42] X. Daura, K. Gademann, B. Jaun, D. Seebach, W. F. van Gunsteren, A. E. Mark, *Angew. Chem. Int. Ed.* **1999**, *38*, 236–240.
[43] W. Humphrey, A. Dalke, K. Schulten, *J. Mol. Graphics* **1996**, *14*, 33–38.
[44] POVRAY, version 3.6, www.povray.org.